AGU PUBLICATIONS

JGR

Journal of Geophysical Research: Space Physics

RESEARCH ARTICLE
10.1002/2015JA021438

Key Points:
- Fringe field can form the ascending structure in the valley region
- The fringe field effect is confined to ±5° latitude
- It explains the occurrence and nonoccurrence of valley region structures

Correspondence to:
E. A. Kherani,
esfhan.kherani@inpe.br

Citation:
Kherani, E. A., and A. K. Patra (2015), Fringe field dynamics over equatorial and low-latitude ionosphere: A three-dimensional perspective, *J. Geophys. Res. Space Physics*, *120*, 6941–6947, doi:10.1002/2015JA021438.

Received 7 MAY 2015
Accepted 20 JUL 2015
Accepted article online 25 JUL 2015
Published online 17 AUG 2015

Fringe field dynamics over equatorial and low-latitude ionosphere: A three-dimensional perspective

E. A. Kherani[1] and A. K. Patra[2]

[1] Aeronomy Division, National Institute for Space Research, São José dos Campos, Brazil, [2] National Atmospheric Research Laboratory, Gadanki, India

Abstract This paper presents a three-dimensional simulation of the collisional interchange instability generating equatorial plasma bubble (EPB) in the evening ionospheric *F* region and associated fringe field (FF) in the valley-upper-*E* (*VE*) region. This simulation is primarily intended to address hitherto unexplained radar observations of ascending irregularity structures only in the vicinity of the magnetic equator in association with the EPB phenomenon. Novel results of the present simulation are the following: (1) EPB-associated FF penetrating into the *E* region is found to be confined to a latitude belt of ±5°, (2) ascending irregularity structures from the *E* region is formed only when perturbation in plasma parameters similar to those responsible for forming EPB are present in the *VE* region, and (3) perturbation in the *VE* region provide conditions for the formation of ascending irregularity structures on the eastern wall of the plasma bubble. These results are in excellent agreement with radar observations and also account for the presence of metallic ions in the EPB at and above the *F* region peak.

1. Introduction

The Valley-upper-*E* (*VE*) region of the ionosphere, a region between 120 and 180 km, hosts varieties of twilight-to-nighttime irregular structures such as the equatorial large-scale ascending, descending and quasi-periodic structures, and off-equatorial descending structures [e.g., *Kelley et al.*, 1981; *Woodman and Chau*, 2001; *Patra et al.*, 2002; *Chau and Hysell*, 2004; *Yokoyama et al.*, 2005; *Patra and Rao*, 2007; *Kherani et al.*, 2012]. Ascending irregularity structures, however, have been observed only at latitudes close to the magnetic equator and during the growth phase of overhead equatorial plasma bubble (EPB) [*Kelley et al.*, 1981; *Woodman and Chau*, 2001; *Kherani et al.*, 2012]. Such rising structures are believed to be the manifestation of the underlying vertical coupling between the *VE* and *F* regions.

The nature of underlying mechanism that sets up such vertical coupling remains an unresolved issue though the fringe field (FF) associated with EPB has been proposed to be a plausible mechanism for the structures observed during the presence of overlying EPB [*Woodman and Chau*, 2001; *Kherani et al.*, 2004]. The concept of FF in EPB is analogous to that of a parallel-plate capacitor where the two walls (eastern and western walls) of the EPB are considered as conducting plates and the low density plasma inside the EPB, which is less conducting, as dielectric. The bottom end of the EPB is located at the base of the *F* layer, which is considered to be one end of the plate capacitor, below which plasma density is low and fringe field would exist in this region due to the polarization changes on the two walls of the EPB. Numerical simulation of EPB has revealed that FF associated with EPB can penetrate down to the upper *E* region and can significantly perturb *VE* region density [*Kherani et al.*, 2004]. However, this simulation study did not attempt to further explore the possibility for the formation of the ascending structures that require the convection of the perturbed *VE* region density structures towards the *F* region. Furthermore, simulations have been performed in the equatorial plane, and it is not known how FF works at latitudes away from the magnetic equator.

Observational studies have also revealed that while these ascending structures are observed in the close vicinity of the equator during the growth phase of overhead EPB [e.g., *Kelley et al.*, 1981; *Woodman and Chau*, 2001], they are not observed in every EPB event. Further, over São Luís, an equatorial location in Brazil, occurrence of these structures were found to decrease from 2002 to 2010 during which the geomagnetic equator remarkably drifted away from São Luís [*Kherani et al.*, 2012]. This finding is remarkable since it indicates the potential role of the magnetic field geometry (i.e., horizontal geometry of Earth's magnetic field) in the vertical coupling between the *F* region and the *VE* regions. Nonoccurrence of these structures with the drifting away of the

geomagnetic equator from São Luís is very similar to the nonoccurrence of these structures over Gadanki [*Patra and Rao*, 2007].

In an attempt to account for the occurrence (nonoccurrence) of the ascending irregularity structures at the equator (off equator), in a recent study, *Mukherjee and Patra* [2014] have developed a three-dimensional FF formalism based on the parallel-plate capacitor analogy of the EPB that is embedded in vacuum. Their study shows a decrease in the capacitor efficiency to generate FF with increasing lateral distance from the equator (i.e., a few degrees north/south of the magnetic equator). While this study has provided a direction in understanding the underlying processes, to understand the latitudinal variation of the FF in a highly anisotropic and altitude varying conductivity scenario such as in the ionosphere, a dynamical simulation of the EPB is desired. Also, the fact that every EPB event does not accompany ascending structures in the *VE* region suggests the need of additional requirements, which may vary from one event to the other. In this study, we employ a three-dimensional simulation model of EPB to investigate the latitudinal variation of FF. We also address how the new simulation results could account for most of the *VE* region features observed during EPB from Jicamarca and São Luís.

2. Simulation Model

Kherani et al. [2005] have developed a three-dimensional (altitude-longitude-latitude) simulation model of the collisional interchange instability (CII), a mechanism that generates EPB. This model has been further upgraded by including the inertial dynamics and has been employed to explain the observed EPB dynamics in the equatorial-low-latitude ionosphere over Brazil [*Abdu et al.*, 2014]. The model solves the following hydromagnetic equations in the ionosphere:

$$\frac{\partial \vec{u}_s}{\partial t} = \frac{q_s}{m_s}(\vec{E} + \vec{u}_s \times \vec{B}) - \nu_s \vec{u}_s + \nu_s \vec{W}, \tag{1}$$

$$\frac{\partial n_s}{\partial t} + \nabla.(n_s \vec{u}_s) = P - L, \tag{2}$$

$$\vec{J} = \underline{\sigma}.\vec{E} + \vec{J}_w; \quad \vec{J}_w = e(n_i \vec{u}_i - n_e \vec{u}_e), \tag{3}$$

$$\nabla.\vec{J} = 0 \quad \text{or} \quad \nabla.(\sigma.\vec{E} + \vec{J}_w) = 0 \quad \Rightarrow \nabla.\vec{E} = -\sigma^{-1}(\vec{E}.\nabla\sigma + \nabla.J_w). \tag{4}$$

$$\vec{E} = \vec{E}_o - \nabla\phi$$

In equations (1)–(4), $(n_s, \vec{u}_s)$ are the ionospheric number density and velocity of species 's' (= *i* for ions and *e* for electron), $(\vec{E}, \phi)$ are the electric field and electrostatic potential, and $(\vec{W}, \vec{j}_w, \vec{J})$ are the initial wind perturbation, corresponding current density and total current density. Equations (1)–(4) form a closed set of equations to study the temporal and spatial variations of the ionospheric number density (n) and electric field $\vec{E}$ or the electrostatic potential (ϕ). At $t = 0$ corresponding to the local time (18:20 LT), the meridional profile of ambient ionosphere (n_o) and latitudinal-temporal profile of ambient electric field (E_o) are shown in Figures 1a and 1b, respectively.

Equations (1)–(4) are solved numerically using finite-difference method in three-dimensional simulation domain that consists of altitude, latitude, and longitude. The implicit Crank-Nicholson scheme is employed to perform the time integration leading to a matrix equation that is subsequently solved by the successive-over-relaxation method. The magnetic dipole coordinate system (p, q, ϕ) is adopted, where p, q, ϕ represent the coordinates outward normal to the Earth's magnetic field, northward directed parallel to the Earth's magnetic field, and azimuth angle (+*VE* toward west), respectively. The simulation domain consists of 90–890 km in altitude, ±20° in geomagnetic latitude and ±6° in longitude.

3. Results

For analysis, the outward component (W_p) of the wind perturbation (W) has been chosen to have a sinusoidal waveform in longitude having amplitude of 1 m/s and wavelength proportional to 6° in longitude, which is ~600 km. In the latitude direction, no wavelength is chosen, and therefore, the perturbation is uniform with

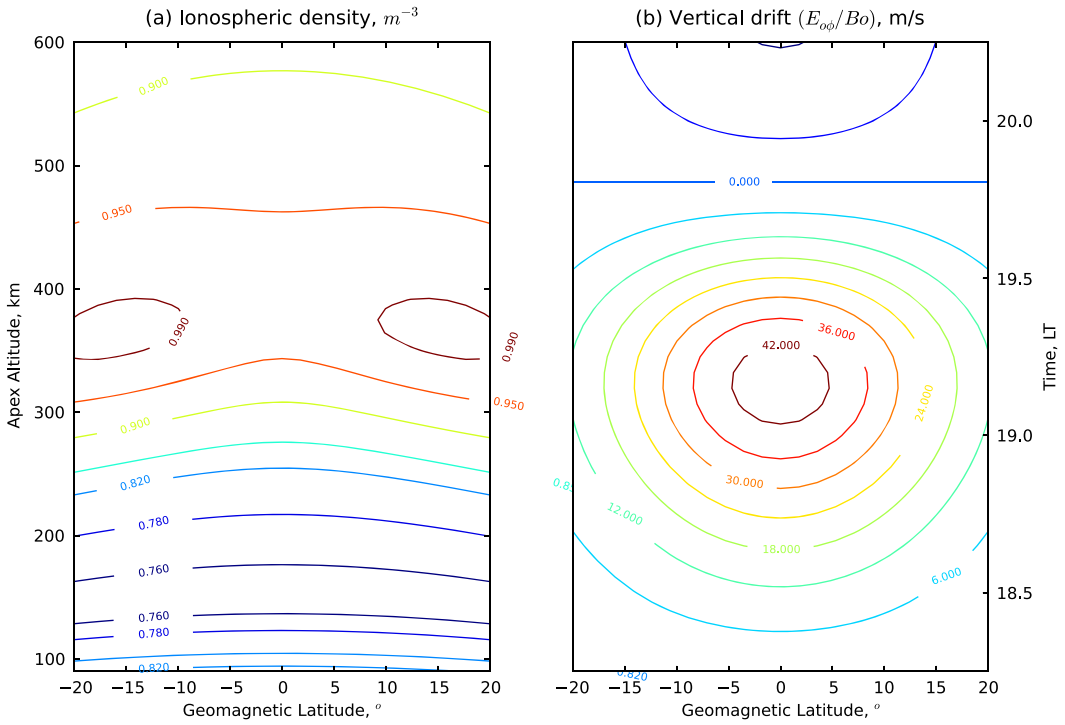

Figure 1. Ambient ionospheric condition: (a) latitude-altitude (meridional) distribution of the ionospheric number density (n_o) and (b) temporal-latitude distribution of the vertical drift ($E_{o\phi}/B_o$). The altitude in Figure 1a represents the apex altitude, and n_o is normalized to the corresponding maximum value ($n_{\max} = 10^{11.8}$).

respect to latitude. Depending on the nature of perturbation in the altitude, two scenarios are considered: (1) Scenario-1 that considers a uniform perturbation in the altitude above 180 km and no perturbation below this altitude and (2) Scenario-2 that considers a uniform perturbation in the altitude both above and below 180 km covering both *VE* and *F* regions.

Scenario-1 was considered in the previous simulation study of FF, which was carried out only for the magnetic equator [*Kherani et al.*, 2004]. The present simulation study includes both equatorial and off-equatorial latitudes under Scenario-1. In addition, the Scenario-2 is added which is a more realistic than the Scenario-1 since, in reality, the initial perturbations, such as those arising from the acoustic-gravity waves, can be present from the lower to upper thermosphere covering the ionosphere from the *VE* region to the *F* region [*Kherani et al.*, 2012].

Electron density (n) and electrostatic potential (ϕ) for the two scenarios are presented in Figures 2 and 3. Figures 2a and 2b depict electron density corresponding to Scenario-1 and Scenario-2, respectively. According to the coordinate chosen here, in these figures, left (right) corresponds to east (west). In these figures, the equatorial distribution of electron density, in the form of isodensity contours (IDCs) for three chosen time, viz., t = 18:20, 19:20, and 20:20 LT. From these figures, we note that IDCs develop significant altitude modulation at 19:20 LT in both scenarios and eventually develop into full blown EPB by 20:20 LT. The IDCs in the *VE* region, however, are different in the two scenarios: the density contours are found to extend down to the *E* region (100 km) in Scenario-2 when compared to those in Scenario-1, where they are limited to the *VE* region (∼150 km).

To demonstrate the variations in electrostatic potential (ϕ), we have chosen results corresponding to t = 20:20 LT for both Scenario-1 and Scenario-2, and the results are shown in Figures 3a and 3b, respectively. Further, potential distributions are shown as normalized electrostatic potential (i.e., $\phi/\phi_{\max}$) in the form of isopotential contours (IPCs). Figure 3 (left and right columns) shows normalized electrostatic potential in the equatorial and meridional planes, respectively. For the meridional plane, we have chosen the longitude of −2.5°, which corresponds to the eastern wall of the depletion. It may be mentioned that in this case, the maximum value of potential ($\phi_{\max}$) at t = 20:20 LT is found to be 75 V. From Figure 3, we note that IPCs with $\phi/\phi_{\max} = -0.06$ belonging to the eastern wall of the EPB penetrate to ∼150 km in Scenario-1, while it

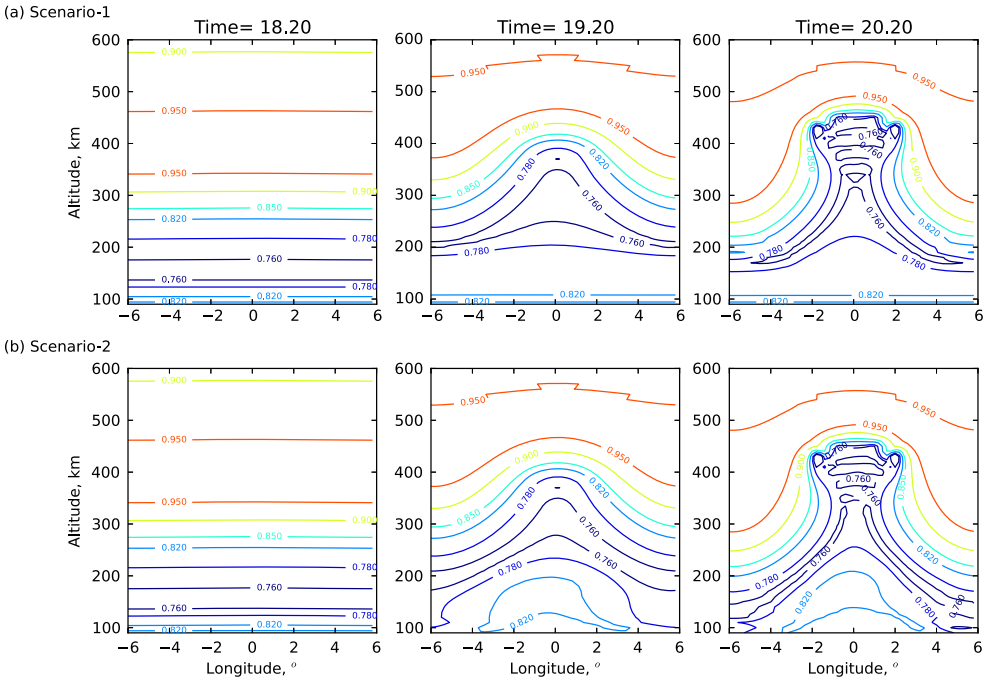

Figure 2. Results from (a) Scenario-1 and (b) Scenario-2: Equatorial distribution of the number density ($n(t)$), in the form of isodensity contours (IDCs), is shown at three selected time t = 18:20, 19:20, 20:20 LT. The number density is normalized to the corresponding maximum value ($n_{max} = 10^{11.8}$); i.e., IDCs of n/n_{max} are shown.

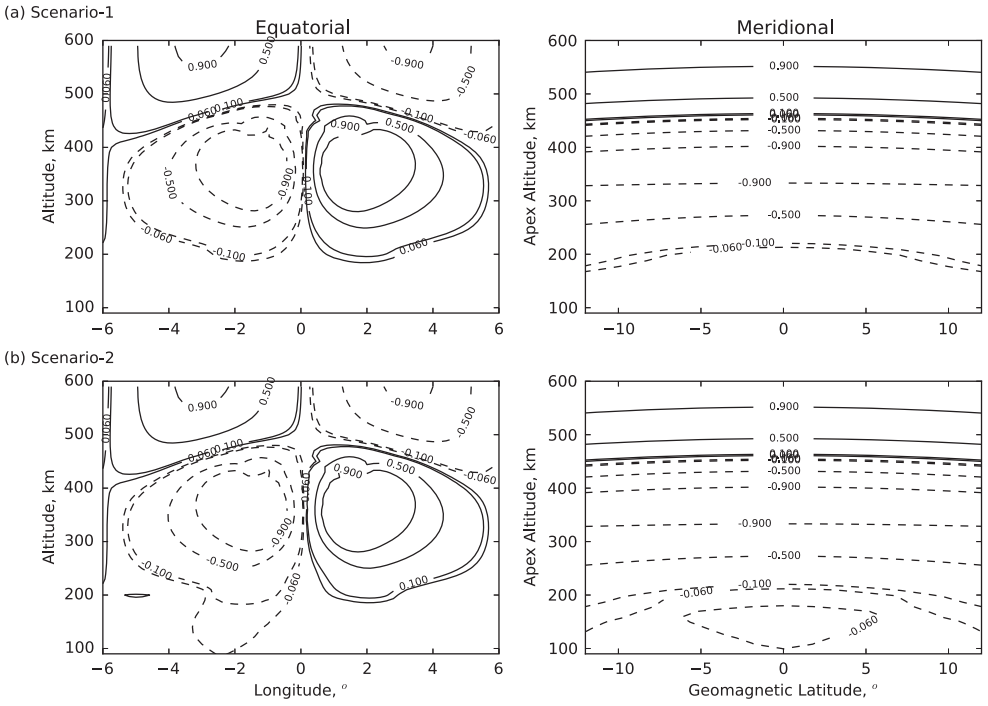

Figure 3. Results from (a) Scenario-1 and (b) Scenario-2: (left column) Equatorial distribution and (right column) meridional distribution of the electrostatic potential ($\phi(t)$), in the form of isopotential contours (IPCs), are shown at the final time t = 20:20 LT. The meridional plane at longitude = −2.5° is chosen that passes through the eastern wall of the EPBs. The potential is normalized to the corresponding maximum value (ϕ_{max} = 60V); i.e., IPCs of ϕ/ϕ_{max} are shown.

penetrates to 100 km in Scenario-2. Interestingly, this penetration is confined within the latitude range ±5°with the maximum penetration being at the equator. Further, in both scenarios, the IPCs originating from the equatorial *F* region are found to be well connected to the *VE* region outside this latitude range, i.e., outside the ±5° latitude belt. This is an indication of mapping of the polarization electric field of the EPB along the magnetic field lines from the *F* region to the *VE* region. Since the bottom of the *F* region over the magnetic equator is connected to the *VE* region over ∼ ±5° latitude due to the geomagnetic field geometry, the mapping of EPB-associated polarization electric field becomes important outside ±5° latitude. Accordingly, the *E* region upward convections by the FF can be clearly seen within ±5° latitude, beyond which polarization electric field associated with EPB dominates.

4. Discussion

From the results presented in section 3, we find that the characteristics of electron density and electrostatic potential distributions noted in Scenario-1 are very similar to those reported in previous simulation study of FF [*Kherani et al.*, 2004]. In such a scenario, FF do causes altitude modulation in electron density in the *VE* region over the equator but does not have any signature down below. In the Scenario-2, however, we note remarkable changes in the potential distribution and so in the electron density. Notably, plasma is found to convect from the *E* region, which has not been reproduced in the earlier simulation of FF. This finding is new and significant considering the fact that such a process would be able to account for the presence of metallic ions in the EPB at altitudes well above the *F* region peak observed by satellite sensors [e.g., *Hanson and Sanatani*, 1971]. The other important result associated with this is that convection of plasma is confined within ±5° magnetic latitude, and the maximum is right over the magnetic equator. Therefore, the simultaneous presence of initial perturbation in the *VE* and *F* regions offers a favorable condition for the convection of the plasma from the *VE* region to the EPB in which this convection is confined to magnetic latitude within ±5°.

As noted in Scenario-2, IPC having $\phi/\phi_{max} = -0.06$ or $\phi = 3.5$ V (since $\phi_{max} = 60$ V) penetrates down to 100 km in the latitude range of ±5°. Noting that the two IPCs with $\Delta\phi \sim 3.5$ V are separated by a distance of ∼50 km vertically and ∼20 km horizontally, the vertical and zonal components of FF become of the order of ∼0.07 mV/m and ∼0.17 mV/m, respectively. Therefore, the FF is mainly horizontal (i.e., zonal) having magnitude less than the ambient electric field, which is in the range of 1–1.5 mV/m. This suggests that plasma from the *VE* region is mainly convected with the ambient zonal electric field with ∼ 15% additional contribution arising from the FF.

It is interesting to note that the IPCs belonging to the eastern wall penetrate much deeper than their western counterpart. This behavior is not observed in Scenario-1, and therefore, the presence of initial perturbation in the *VE* region is responsible for the noted east-west asymmetry in Scenario-2. This asymmetry is owing to the fact that in the *VE* region, contribution to the zonal current, which is the source of free energy for the equatorial CII, is arising from both ions and electrons (or from both Pederson and Hall currents) unlike in the *F* region where contribution is only from ions (or only from Pederson current). To understand this underlying mechanism, we show a sketch in Figure 4 applicable for a chosen *VE* altitude where the Hall conductivity (σ_H) is equal to the Pederson conductivity (σ_P). It is evident that in the presence of ambient eastward electric field as considered in the present study, the eastern and western walls of a depleted region in the *VE* region will have perpendicular field toward east-up and east-down, respectively. Therefore, the ions will have dominant Pederson drift (u_i) in these directions. On the other hand, the electrons will have dominant Hall drift (u_e) perpendicular to these two directions, i.e., in the west-upward and east-downward directions. Therefore, in the eastern wall, the ions and electrons drift in the opposite directions (i.e., eastward and westward, respectively), while in the western wall, they drift in the same direction (i.e., eastward). Therefore, the resulting zonal current, which is the source of free energy for the CII at the magnetic equator, is larger at the eastern wall than at the western wall, providing more favorable condition for the growth of CII at the eastern wall. This leads to the asymmetric IPCs with more potential at the eastern wall.

In the *F* region, the Hall current is negligibly small, and therefore, only Pederson drift of ions participates in the zonal current which is same at both eastern and western walls of the initial depletion, leading to the symmetric IPCs.

4.1. Comparison With the Observations

Three important findings of the present simulation study that are of direct relevance to observations are the following: (1) convection of the *VE* region plasma by FF is confined to magnetic latitudes within ±5°, (2) FF is

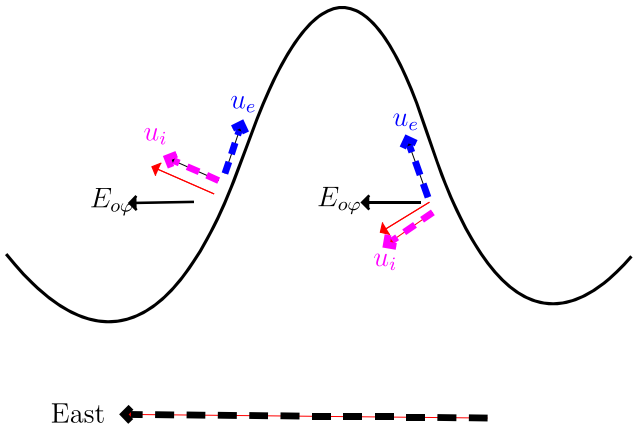

Figure 4. A sketch illustrating electron (u_e) and ion (u_i) velocities, and ambient zonal electric field ($E_{o\phi}$) at an altitude where Pederson conductivity (σ_P) is equal to Hall Conductivity (σ_H). Red arrows represent the directions of electric field component perpendicular to the wall of depletion.

much stronger at the eastern wall than at the western wall of the EPB, and (3) plasma from the *VE* regions is mainly convected by ambient zonal electric field with ~15% additional contribution from FF. The first finding is consistent with the ascending irregularity structures observed over Jicamarca and to some extent over São Luís (as long as the magnetic equator was close to São Luís) [e.g., *Kelley et al.*, 1981; *Woodman and Chau*, 2001; *Kherani et al.*, 2012] and nonoccurrence of such structures over Gadanki and Kototabang [*Yokoyama et al.*, 2005; *Patra and Rao*, 2007]. Coming to the second finding, we may recall that equatorial observations always show rising *VE* structure beneath the eastern wall of EPB [e.g., *Kelley et al.*, 1981; *Woodman and Chau*, 2001]. Thus, the second finding is very much consistent with the preferential eastern surging of the ascending *VE* structures. From observations, we also noted that the ascending *VE* structures drift upward with velocity somewhat larger than the ambient plasma drift [*Woodman and Chau*, 2001]. The third finding seems to support this fact. We found that the observed characteristics of the rising *VE* structures can be accounted for by the three important findings that emerged from the simulation study presented here. Importantly, the present simulation also suggests that perturbation in the *VE* region is important for the manifestation of ascending irregularity structures right from the *E* region in consistent with observations. This implies that for every EPB event ascending plasma structures would not be formed in the absence of perturbation in the *VE* region, which is very much consistent with observations that every EPB event does not accompany with ascending irregularity structures.

4.2. Comparison With the Earlier Theoretical Work

The first finding is broadly consistent with the three-dimensional calculation of FF based on the parallel-plate analogy of EPB in the vacuum performed earlier by *Mukherjee and Patra* [2014]. Penetration of FF in the *VE* region and weakening of FF with latitude were also noted by *Mukherjee and Patra* [2014]. The weakening of FF with latitude, however, was significant at the *E* region. In that sense, results presented by *Mukherjee and Patra* [2014] and those obtained in Scenario-1 in the present study appear to be somewhat similar although there remain some differences, which are related to different approaches adopted in these studies. For example, in Scenario-1 of the present study, simulation has been carried out under the condition of anisotropic/altitude varying conductivity and results show that plasma is convected only from the *VE* region into the EPB. This scenario, however, changed when perturbation is applied in the *VE* and overlying *F* region, resulting in plasma structures right from the *E* region.

5. Summary and Conclusions

In the present study, we have performed three-dimensional simulation of EPB and studied associated FF dynamics in an effort to explain the occurrence (nonoccurrence) of ascending irregularity structures at the magnetic equator (off equator). Results clearly show that FF, which influences the *VE* region and results in ascending irregularity structures, is confined to a latitude belt of ±5°, and this condition is effective when perturbation in the *VE* region is considered. When perturbation in the *VE* region is not included in the simulation, fringe field does perturb the *VE* region but does not result in any ascending irregularity structures. Simulation also shows that fringe field effects are confined to the eastern wall of EPB, a feature which is very much consistent with observations showing that the ascending *VE* structures preferably surge beneath the eastern wall of EPB.

Acknowledgments
Data presented in this paper are available with E. A. Kherani (esfhan.kherani@inpe.br) and can be accessed upon request. This work was supported by INPE and NARL and was carried out while E.A.K. was on a short visit to NARL. The visit of E.A.K. was supported by FAPESP under process 2011/21903-3.

Michael Balikhin thanks two anonymous reviewers for their assistance in evaluating this paper.

References

Abdu, M. A., E. A. Kherani, I. S. Batista, B. W. Reinisch, and J. H. A. Sobral (2014), Equatorial spread F initiation and growth from satellite traces as revealed from conjugate point observations in Brazil, *J. Geophys. Res. Space Physics*, *119*, 375–383, doi:10.1002/2013JA019352.

Chau, J. L., and D. L. Hysell (2004), High altitude large-scale plasma waves in the equatorial electrojet at twilight, *Ann. Geophys.*, *22*, 4071–4076.

Hanson, W. B., and S. Sanatani (1971), Relationship between Fe+ ions and equatorial spread F, *J. Geophys. Res.*, *76*, 7761–7768, doi:10.1029/ JA076i031p07761.

Kelley, M. C., M. F. Larsen, C. LaHoz, and J. P. McClure (1981), Gravity wave initiation of equatorial spread F: A case study, *J. Geophys. Res.*, *86*, 9087–9100.

Kherani, E. A., E. R. de Paula, and F. C. Bertoni (2004), Effects of the fringe field of Rayleigh-Taylor instability in the equatorial E and valley regions, *J. Geophys. Res.*, *109*, A12310, doi:10.1029/2003JA010364.

Kherani, E. A., M. Mascarenhas, J. H. A. Sobral, E. R. de Paula, and F. C. Bertoni (2005), A three dimensional simulation model of collisional interchange instability, *Space Sci. Rev.*, *121*, 253–269.

Kherani, E. A., E. R. de Paula, R. Y. C. Cueva, and L. A. P. Camargo (2012), Observations of nighttime equatorial-upper-E-valley region irregular structures from Sao Luis radar and their occurrence statistics: A manifestation of vertical coupling between E and F regions, *J. Atmos. Sol. Terr. Phys.*, *75*, 64–70, doi:10.1016/j.jastp.2011.08.017.

Mukherjee, S., and A. K. Patra (2014), Parallel plate capacitor analogy of equatorial plasma bubble and associated fringe fields with implications to equatorial valley region irregularities, *J. Geophys. Res. Space Physics*, 6631–6641, doi:10.1002/2014JA020113.

Patra, A. K., and N. V. Rao (2007), Low-latitude valley region irregularities studied using the Gadanki radar, *J. Geophys. Res.*, *112*, A03303, doi:10.1029/2006JA011857.

Patra, A. K., P. B. Rao, V. K. Anandan, A. R. Jain, and G. Viswanathan (2002), Evidence of intermediate layer characteristics in the Gadanki radar observations of the upper E region field-aligned irregularities, *Geophys. Res. Lett.*, *29*(14), 1696, doi:10.1029/2001GL013773.

Woodman, R. F., and J. L. Chau (2001), Equatorial quasiperiodic echoes from field-aligned irregularities observed over Jicamarca, *Geophys. Res. Lett.*, *28*, 207–209, doi:10.1029/2000GL000076.

Yokoyama, T., A. K. Patra, S. Fukao, and M. Yamamoto (2005), Ionospheric irregularities in the low-latitude valley region observed with the Equatorial Atmosphere Radar, *J. Geophys. Res.*, *110*, A10304, doi:10.1029/2005JA011208.